An Analysis of an ICRF Antenna with Controllable Toroidal Wavenumber in LHD

Hiroshi KASAHARA, Tetsuo SEKI, Kenji SAITO, Ryuhei KUMAZAWA, Takashi MUTOH, Fujio SHIMPO and Goro NOMURA

National institute for fusion science, 322-6 Oroshi-cho, Toki 509-5292, Japan

(Received 9 December 2009 / Accepted 28 April 2010)

In order to excite fast wave in the ion cyclotron range of frequencies (ICRF) using multiple antennas with the phase difference in the Large Helical Device (LHD), a controllable wavenumber antenna that consists of two single-strap antennas is designed, and the electrical characteristic features of the antenna are estimated by using a three-dimensional electromagnetic commercial code and the simplified antenna model. Controlling the radio-frequency (RF) phase difference between these two single-straps, reverse-phase excitation can be achieved in order to reduce the impurity production. According to this estimate, the RF current profile on the strap surface is strongly concentrated on the both horizontal strap edges, and the electrical strap length at frequency of 85 MHz is longer than the quarter wavelength of 85 MHz ($\lambda_{85\,\mathrm{MHz}}/4$). Excitable wavenumber spectra are different in various RF phases and frequencies. At the low frequencies (< 60 MHz) with in-phase, effective wavenumbers between $k = 0\,m^{-1}$ and $k = 10\,m^{-1}$ can be excited. During the reverse-phase excitation, large ($k = 6,\ 15\,m^{-1}$) wavenumber spectra with low ($k = 0\,m^{-1}$) wavenumber kept small are obtained.

Keywords: ICRF, three-dimensional calculation, fast wave, wave excitation, helical plasma, antenna modeling, antenna loading

DOI: 10.1585/pfr.5.S2090

1. 1. Introduction

In order to achieve steady-state operation in fusion reactor, various heating methods have been studied in torus plasmas, and radio-frequency (RF) heating using ion cyclotron range of frequencies (ICRF) is one of the attractive heating methods for the realization of fusion. Many heating operations using fast wave in ICRF have been studied, and minority heating (MH) [1, 2], 2nd harmonics heating (2nd) [3], mode-converted ion Bernstein wave heating (MC-IBW) and higher harmonics fast wave heating (HHFW) [4] have been developed in the Large Helical Device (LHD) [5].

MH has a favorable heating efficiency with low impurity production in the LHD, and a long discharge, with a duration time of 54 min. and 28sec., is demonstrated using MH and electron cyclotron heating (ECH) support [5]. One-pair superconducting helical coils make the magnetic surface in the LHD, and there is no need to produce plasma current to achieve steady-state discharge as in tokamaks. As a consequence of plasma current-less operation, the long-pulse operation using ICRF is usually stable, any instability is quasi-silent. Nevertheless, a critical issue is left in steady-state operations, which is that abrupt impurity productions prevent plasma from being maintained for a long time due to radiation collapse. At this time local hot spots and many sparks were observed by CCD camera just before the large impurity penetration, and the spark frequency gradually increased. By reducing the temperature of local hot spots on the divertor plate, the plasma discharge time was extended [6]. Since local hot spots are close to the impact points of accelerated particles in front of the ICRF antenna, sheath loading is one of the causes of local hot spots. In tokamak ICRF experiments, reverse-phase excitation using multiple straps was useful to reduce sheath loading, and the reduction of hot spots was observed [7, 8].

The reverse-phase excitation is carried out using the phase difference between two straps of a new designed ICRF antenna, and the new ICRF antenna, which is a controllable toroidal wavenumber to magnetic field line, has been designed (see Fig. 1). In section 2, a clear difference between the newly designed and the present ICRF antenna is shown, and in section 3 the electrical characteristic features of the new ICRF antenna are calculated using a three-dimensional electromagnetic commercial code (high frequency structure simulator, HFSS™ [9]). In this section, unbalanced antenna loading and excitable spectra are shown for various frequencies and phase differences. Finally we summarize and discuss the new ICRF antenna in the LHD in section 4.

2. A Newly Designed ICRF Antenna in the LHD

Figure 1 shows the newly designed ICRF antenna,

author's e-mail: kasahara.hiroshi@LHD.nifs.ac.jp

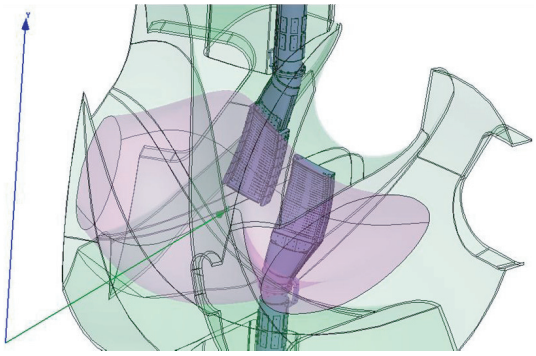

Fig. 1 The newly designed ICRF antenna is shown. There are two single-strap antennas (U and L antenna), and these antenna shapes are the same. Each antennas can independently move along the radial direction of the plasma (violet), and the parallel wavenumber can be controlled using the phase difference between these straps.

which consists of two single-strap antennas, which can move separately along the radial direction to control the distance between the plasma and these antennas. These single-strap shapes are the same, and they are approximately fitted on the magnetic surface. These antennas are located along the minor axis of the helical plasma, and the antenna can excite various wavenumbers using the phase difference ($\Delta\theta$) between these straps. When the phase difference reaches zero, reverse-phase excitation is achieved. In the case of the present ICRF antenna in the LHD, the ICRF antenna was installed from the upper port (U-port) and the lower port (L-port), and these antennas were vertically installed to the equatorial plane of the LHD. The angle of these straps was not perpendicular to the magnetic field line. The Faraday-shield of the present antenna has an angle of 12° to the equatorial plane, and the straps of the present antenna were not perpendicular to the magnetic field line. In order to excite ideal fast wave to heat plasmas, the straps of the new ICRF antenna are designed to be in a matched vertical location to the magnetic field line in front of the antenna surface, and then the Faraday-shield angle is just vertical to the current strap. According to HFSS calculation using the actual present ICRF antenna model, RF current on the strap surface is strongly concentrated on both strap edges along the magnetic field line, and RF current is largest at the connection point of the strap to the bottom plate. Since the intensity of excited fast wave is strongly related to the RF current on the strap surface, the largest RF current positions of new ICRF antenna are close to each other such as shown in Fig. 1.

With the new ICRF antenna design, we aim at high density ($> 10^{21}$ m^{-3}) and high beta plasma heating through electron Landau damping (ELD) and transit-time magnetic pumping (TTMP), and the fast wave with large wavenumber, which is more easily excited by the new antenna with the reverse-phase than with the present antenna, is capable of heating the plasma center with high electron beta. In order to excite the wave with large wavenumber without arching between these antennas, the distance between the U-port antenna (left) and the L-port antenna (right) is short (~ 10 cm). The distance is not optimized to achieve an efficiency of electron heating using ELD and TTMP for high power RF injection.

3. Characteristic Features of Newly Designed ICRF Antenna Using a Simplified Antenna Model

The commercial three-dimensional code HFSS, is a powerful solver to calculate an RF field with a complicated geometry, and the calculation results of the present ICRF antenna are well matched to experimental results [10]. At the same time a large calculation and a large working memory absolutely necessary, and it requires a great investment of time to calculate the actual complicated mode in various conditions. According to comparison of the actual present antenna model with a simplified antenna model, which is a squared board model, an antenna loading with large permittivity material in front of the ICRF antenna and an excited magnetic field around the antenna are roughly the same [11], and the simplified model is very useful for reducing the calculation time in various surveys. The simplified antenna model is one of the candidates to be used in studying an antenna loading and an excited RF field around the ICRF antenna, and a large permittivity material as imaginary plasma has been studied using several solvers [12–14]. A relative permittivity of approximately a few thousand as an imaginary plasma is suitable for an actual plasma model which is similar to a typical JET ELMy H mode plasma [14].

Figure 2 (a) shows the simplified new antenna model, and Fig. 2 (b) shows typical antenna sizes and distances of this model. This antenna is located in the vacuum region, and a perfect conductor is put behind the back-plate of the antenna as a metal wall. As a loading material instead of plasma, a large permittivity material (ε ~2000) [13, 14] is placed in the vacuum region in front of the antenna, and the size of the large permittivity material is as follows; $\Delta x = 10$ cm, $\Delta y = 2$ m and $\Delta z = 2$ m. In this model, the y-direction of this figure matches the direction of magnetic field, and the calculated region is significantly larger than the size of the antenna. The total calculated region is $\Delta x = 23$ cm, $\Delta y = 2$ m and $\Delta z = 2$ m, and boundaries of the calculation region except the metal wall are radiative and non-reflective.

Figure 3 shows the amplitude of the excited magnetic field to the y-direction over the strap surface with frequencies of 28.4 MHz and 85 MHz, and they indicate RF current on the strap surface, which is proportional to the excited magnetic field. There are some marks, "left" and "right" in this figure, and they show the end of the strap to the y-direction. RF power is supplied from the top of the frame in this figure, and the strap is connected to the

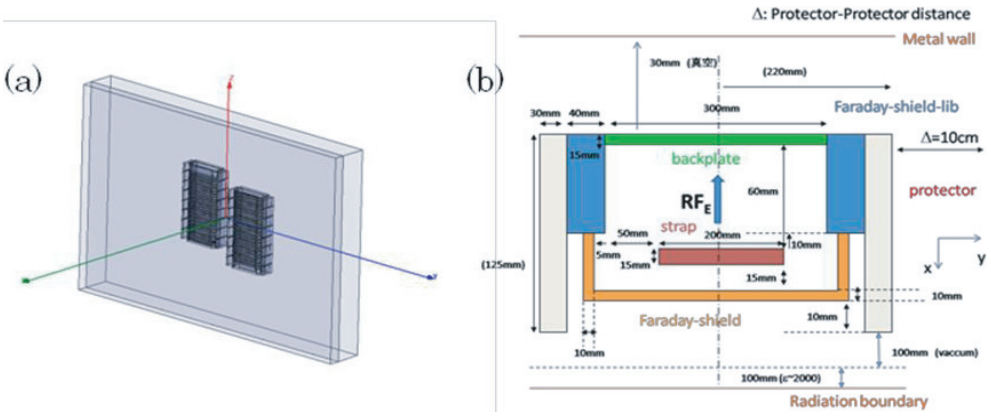

Fig. 2 The simplified squared antenna model. The typical significant distances are as follows; the distance of the back plate- the wall ~ 3 cm, the distance of the protector- the imaginary load (between the antenna protector and large permittivity material) ~ 10 cm and the distance of the left antenna- the right antenna ~ 10 cm.

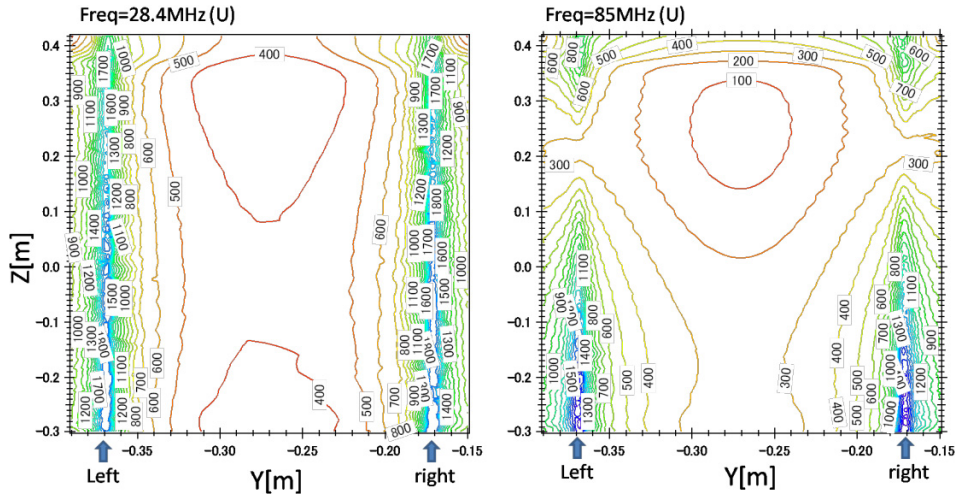

Fig. 3 RF current profiles on the strap surface in the reverse-phase excitation at the frequency of 28.4 (left) and 85 MHz (right). These RF current profiles are similar to those in the in-phase excitation. RF supply port is located at the top of this frame ($Z \sim 0.5$ m), and the antenna strap is connected to the bottom plate at the bottom of the frame ($Z \sim -0.3$ m). The RF current is strongly concentrated on both the strap edges ('left' and 'right' is the edge of the strap). The RF current profile of the strap edges is clearly observed in the frequency of 85 MHz.

bottom plate at the end of the frame of this figure. The RF current is strongly concentrated on the both strap edges to the y-direction, and it suggests that the ohmic loss of the strap edge is twenty times larger than that of the center of the strap. For steady-state operation, the heat removal mechanism of the ohmic loss is important of the edge of the strap. As the excited RF frequency is increased from 28.4 MHz to 85 MHz, small current region appears at the edge of strap around z of 0.2 m at the frequency of 85 MHz. Since this antenna geometry along to z-direction is the same, the shortening effect on the strap surface seems to be uniform. If the shortening effect of the wavelength for the profile on the strap surface is constant, the shortening effect (η_{short}) can be estimated using equation (1). The RF current is minimized at the quarter wavelength, and the shortening effect is approximately 0.5/0.88 (~ 0.57).

$$\eta_{\text{short}} = L(0.5\,\text{m})/(\lambda_{85\,\text{MHz}}/4) \approx 0.57. \quad (1)$$

where $\lambda_{85\,\text{MHz}}/4 = 0.88$ m.

According to the RF magnetic calculation, an optimum frequency of this antenna model exists from 28.4 MHz to 85 MHz, and the optimum frequency at which strap length is consistent with the quarter wavelength including shortened effect is approximately 60 MHz.

Figure 4 shows the antenna loading in various frequencies with various phase differences, and these antenna loadings are matched to each other at the in-phase ($\Delta\theta = 0°$) and the reverse-phase ($\Delta\theta = 180°$) excitations. By changing the L-port phase with the U-port phase kept constant, the phase difference is produced, and voltage standing wave ratios (VSWR) of both RF injection ports are calculated at the same time. After that antenna loading

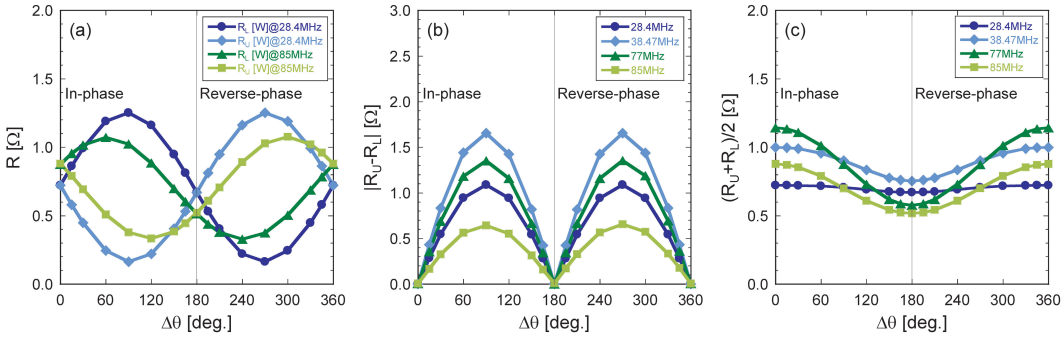

Fig. 4 Antenna loadings in various frequencies and phase differences $\Delta\theta$ between U-port and L-port RF power injection. In Fig. 4 (a) and 4 (b), the difference of antenna loadings between U and L ($|R_U - R_L|$) are large as $\Delta\theta$ is increased, and the difference are negligible in the in-phase ($\Delta\theta = 0°$) and the reverse-phase ($\Delta\theta = 180°$) excitation. Both antenna loadings, R_U and R_L, have periodicity, and the periodicity of the phase difference is just 180°. Figure 4 (c) shows the averaged antenna loadings, and large antenna loading is achieved in the in-phase excitation and the small antenna loading is achieved in the reverse-phase excitation.

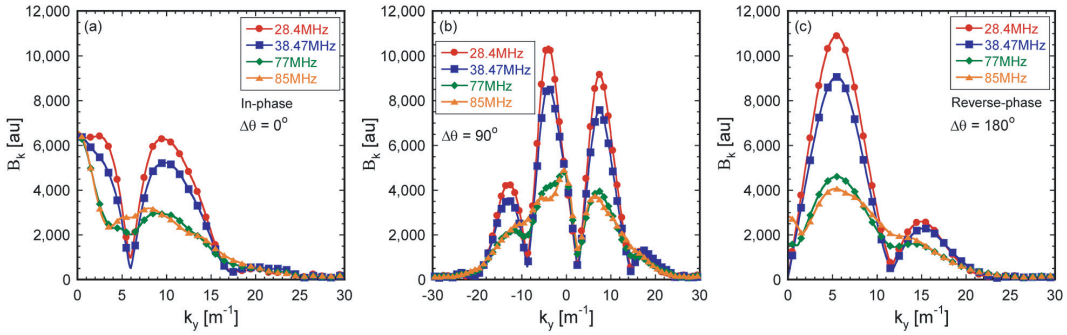

Fig. 5 Excited wave spectrum (B_k) which is integrated on the given plane around the imaginary load ($x_0 = 9.9$ cm) in three phase differences and frequencies. In the in-phase(a) and the reverse-phase(c) excitation, symmetric spectra are obtained in positive and negative wavenumber, and in the phase difference $\Delta\theta$ of 90° ($\Delta\theta = 90°$) the asymmetric spectrum is shown in Fig. 6 (b). In the in-phase excitation, effective excited wavenumbers are approximately the k_y of 0 m^{-1} and ± 10 m^{-1}, and in the reverse-phase excitation those are approximately ± 5 m^{-1} and ± 15 m^{-1}. In the $\Delta\theta$ of 90° excitation, major three excited wavenumbers are 7 m^{-1}, -4 m^{-1} and -13 m^{-1}, and at higher frequencies (> 60 MHz) the broad spectrum is observed.

is estimated by a relational expression, $R = 50/\mathrm{VSWR}[\Omega]$. These antenna loadings of U-port (R_U) and L-port (R_L) are the same in the in-phase ($\Delta\theta = 0°$) and the reverse-phase ($\Delta\theta = 180°$) excitations in Fig. 4 (a)-(b), and there are differences of the antenna loadings in the other phase excitations. As the phase difference is increased from $\Delta\theta = 0°$ to $\Delta\theta = 90°$, unbalanced antenna loading is extended in all frequencies in Fig. 4 (b). In order to estimate the actual antenna loading from both the antennas, these averaged antenna loadings (R_U+R_L)/2 are shown in Fig. 4 (c), and the averaged antenna loading at the frequency of 28.4 MHz is roughly constant in various phase differences. On the other hand, the average loading at the frequency of 77 MHz has a large difference in various phase differences. In all cases, these averaged antenna loadings in the in-phase excitation are larger than those in the reverse-phase excitation, and that seems to be the excitable wavenumber.

Figure 5 shows the total excited spectra B_k with a supplied RF power of 1 MW from a port in various frequencies on the yz-pane with the distance X_0 of 9.9 cm between the plane and the antenna, and there are three kinds of the phase difference; (a): $\Delta\theta = 0°$, (b): $\Delta\theta = 90°$ and (c): $\Delta\theta = 180°$. In the in-phase excitation (a), the spectra with low wavenumber are easily excited, and the spectra with large wavenumber are relative largely excited at low frequencies (< 60 MHz). The intensity of the k_y of 10 m^{-1} is similar to that of 0 m^{-1}, and there are two target electron temperatures for ELD and TTMP. The lower target electron temperature (k_y of 10 m^{-1}) in the frequency of 38.47 MHz is a few hundred eV, since the large up-shift is achieved through the propagation in the LHD plasma. In the case of a $\Delta\theta$ of 90°, the B_k profile is asymmetric, and strong spectrum peaks are obtained around the k_y of 7 m^{-1}, -4 m^{-1}, -13 m^{-1} in low frequencies excitation. Two spectrum peaks around k_y of 0 m^{-1} and 7 m^{-1} are observed in the high frequencies (77 MHz and 85 MHz), and their spectrum profiles are broad from -25 m^{-1} to 25 m^{-1}. Figure 5 (c) shows the reverse-phase excitation spectrum, and the spectrum with the large wavenumber can be excited with the low wavenumber being kept small. Under the fre-

quency of 60 MHz, the spectra have a strong peak around k_y of 5 m^{-1}, and the peaked intensity of the spectrum in the reverse-phase is 1.8 times larger than that in the in-phase.

4. Summary and Discussion

A new ICRF antenna for the LHD has been designed, and it consists of two single-strap antennas. The antenna is set up along the magnetic field in Fig. 1, and a fast wave can be excited using these two straps with the phase difference in order to carry out the reverse-phase excitation. According to the three-dimensional electromagnetic analysis using HFSS, the RF current is strongly concentrated on the both strap edges (Fig. 3), and the RF current profile on edges of the strap isn't uniform at the frequency of 85 MHz. A small RF current region appears at $z = 0.2$ m, and the strap length is longer than the quarter electrical length. If the shortening effect is constant on the strap surface in various frequencies, the maximum antenna loading can reach a frequency of around 60 MHz. At this time the length of the strap is just close to the quarter wavelength including the shortening effect. This assumption is consistent with the calculation result of the averaged antenna loading with the $\Delta\theta$ of 0° in Fig. 4 (c), and the largest antenna loading is achieved at the frequency of 77 MHz, which is the closest frequency to the quarter wavelength. The actual antenna bends according to the helical plasma shape, and it is necessary to use these calculation results carefully because this calculation model does not include the bending effect. In order to carry out the reverse-phase excitation, the new ICRF antenna has a controllable mechanism of the phase difference, and operation with phase difference is achieved without a decoupler in the in-phase and the reverse-phase excitation, in which the antenna loadings of the two straps are the same. Target electron temperature using ELD and TTMP is strongly related to the excited wavenumber, and the temperature can be selected by controlling the phase difference. Comparing the spectra of the in-phase with that of the reverse-phase, large wavenumber is more easily excited in the in-phase operation than in the reverse-phase operation, but the intensity of the large wavenumber of the reverse-phase is 1.8 times larger than that of the in-phase, as in Fig. 5 (a)-(c). In order to achieve the targeted low electron temperature, this antenna model should be slimer than the present ICRF antenna, and the target electron temperature in the in-phase is a few thousand eV at the frequency of 38.47 MHz. In order to study more accurately antenna loading and the excited spectrum, we have to calculate using the actual new ICRF antenna model, and the new ICRF antenna modeling has been promoted. The actual antenna calculation using the new ICRF antenna model is a future task, and we will study the permittivity effect using a multi-layer material in order to realize the profile of electron density at that time.

Acknowledgments

This work was partially supported by a budgetary Grant-in-Aid NIFS09ULRR525 from the National Institute for Fusion Science.

[1] T. Mutoh, R. Kumazawa, T. Seki, T. Watari, K. Saito *et al.*, Phys. Rev. Lett. **85**, 4530 (2000).
[2] R. Kumazawa, T. Mutoh, T. Seki, T. Watari, K. Saito, Y. Torii *et al.*, Phys. Plasmas **8**, 2139 (2001).
[3] K. Saito, R. Kumazawa, T. Mutoh, T. Seki, T. Watari *et al.*, Nucl. Fusion **41**, 1021 (2001).
[4] H. Kasahara, T. Oosako, Y. Takase, N. Takeuchi, K. Saito *et al.*, J. Korean Phys. Soc. **49**, S192 (2006).
[5] O. Motojima, H. Yamada, A. Komori, N. Ohyabu, T. Mutoh *et al.*, Nucl. Fusion **47**, S668 (2007).
[6] R. Kumazawa, T. Mutoh, K. Saito, T. Seki, H. Kasahara *et al.*, *Proceeding of 22th IAEA Fusion Energy Conference* (2008), IAEA-EX/P6-29.
[7] J. R. Myra, D. A. D'Ippolito, D. A. Russell, L. A. Berry, E. F. Jaeger and M. D. Carter, Nucl. Fusion **46**, S455 (2006).
[8] S. J. Wukitch, B. Labombard, Y. Lin, B. Lipschultz, E. Marmar, M. L. Reinke and D. G. Whyte, J. Nucl. Mater. **390-391**, 951 (2009).
[9] HFSS™, *IEEE MTT-S International Microwave Symposium*, Honolulu, USA, June 5 (2007).
[10] T. Mutoh *et al.*, "Elctromagnetic field simulation for ICRF antenna and comparison with experimental results in LHD", ITC19th (2009).
[11] K. Saito *et al.*, *Annual Report of National Institute for Fusion Science April 2008-March 2009*, 120 (2009).
[12] V. Bobkov *et al.*, J. Nucl. Mater. **390-391**, 900 (2009).
[13] H. Bosttollier-Curtet, M. EI Khaldi *et al.*, 25th *Symposium on Fusion Technology, Rostock, Germany* (2008).
[14] P. U. Lamalle *et al.*, Nucl. Fusion **46**, 432 (2006).